Enhanced Strong Interaction between Nanocavities and *p*-shell Excitons Beyond the Dipole Approximation

Chenjiang Qian,[1,2] Xin Xie,[1,2] Jingnan Yang,[1,2] Kai Peng,[1,2] Shiyao Wu,[1,2] Feilong Song,[1,2] Sibai Sun,[1,2] Jianchen Dang,[1,2] Yang Yu,[1,2] Matthew J. Steer,[3] Iain G. Thayne,[3] Kuijuan Jin,[1,2] Changzhi Gu,[1,2] and Xiulai Xu[1,2,4,*]

[1]*Beijing National Laboratory for Condensed Matter Physics, Institute of Physics, Chinese Academy of Sciences, Beijing 100190, China*

[2]*CAS Center for Excellence in Topological Quantum Computation and School of Physical Sciences, University of Chinese Academy of Sciences, Beijing 100049, China*

[3]*School of Engineering, University of Glasgow, Glasgow G12 8LT, United Kingdom*

[4]*Songshan Lake Materials Laboratory, Dongguan, Guangdong 523808, China*

(Received 6 September 2018; published 27 February 2019)

Large coupling strengths in exciton-photon interactions are important for the quantum photonic network, while strong cavity–quantum dot interactions have been focused on *s*-shell excitons with small coupling strengths. Here we demonstrate strong interactions between cavities and *p*-shell excitons with a great enhancement by the *in situ* wave-function control. The *p*-shell excitons are demonstrated with much larger wave-function extents and nonlocal interactions beyond the dipole approximation. Then the interaction is tuned from the nonlocal to the local regime by the wave function shrinking, during which the enhancement is obtained. A large coupling strength of 210 μeV has been achieved, indicating the great potential of *p*-shell excitons for coherent information exchange. Furthermore, we propose a distributed delay model to quantitatively explain the coupling strength variation, revealing the intertwining of excitons and photons beyond the dipole approximation.

DOI: 10.1103/PhysRevLett.122.087401

Strong interactions between single photons and excitons in nanocavities play a central role in the quantum photonic network [1,2]. The control and enhancement of exciton-photon interaction is significant for improving the efficiency and fidelity of the coherent control in quantum information processing [3–5]; thus the large coupling strength is always pursued in cavity quantum electrodynamics (CQED). Additionally, the control of coupling strength also provides the base for the study of many other exciton-photon interactions, such as exceptional points and topological polaritons [6–8].

As an ideal material for the solid-state quantum photonic network, quantum dots (QDs) embedded in photonic crystal cavities provide exciton-photon polariton states with a long coherence time and chip-scale integrability. However, previous investigations are mainly focused on the *s* shell (ground state) with the dipole approximation (DA) uncritically adopted, limiting the coupling strength g to a small value with low controllability [9]. The enhancement and control of g by tuning the cavity mode or moving the emitter, which is valid for some specific materials [10–13], requires complex mechanical controls and is unrealistic for the solid-state cavity-dot system. By contrast, the wave-function control by an external magnetic field can control the exciton-photon interaction *in situ* [14–16], but only a small decrease of g has been obtained on the *s* shell with the DA [16–18].

Here we demonstrate the significant nonlocal interaction beyond the DA in the *p*-shell (excited state of QDs) cavity system, which has a wave-function extent much larger than the *s* shell. The *in situ* wave-function control is applied to tune the interaction from a nonlocal to a local regime. During the phase transition, the cavity-dot coupling strength is greatly enhanced, with a largest value of 210 μeV achieved so far. The enhancement is quantitatively explained by a new phenomenological distributed delay model, which extends the local interaction in the former monotonic decrease model [16] to the nonlocal interaction as a nontrivial intertwining of excitons and photons beyond the DA. Therefore, our work opens up a new area of excited states in QD-based CQED with great significance to the solid-state quantum photonic network.

For the exciton-photon interaction between a quantum emitter with transition energy $\omega_x = \omega_f - \omega_i$ from the initial state $|i\rangle$ to the final state $|f\rangle$, and a quantized radiation field with cavity-mode wave function $\boldsymbol{\alpha}(\boldsymbol{r})$ [Fig. 1(a)], the perturbation theory gives the coupling strength g proportional to $|\langle f|\boldsymbol{\alpha}(\boldsymbol{r})\cdot\boldsymbol{p}|i\rangle|$, where $\boldsymbol{p}$ is the momentum operator. As $\boldsymbol{\alpha}(\boldsymbol{r})$ is untunable for a solid-state nanocavity, the wave-function control on $|i\rangle$ and $|f\rangle$ is the only approach to the enhancement and control of g. For quantum emitters, the wave function can be modified by an external magnetic field. The magnetic field adds an additional lateral

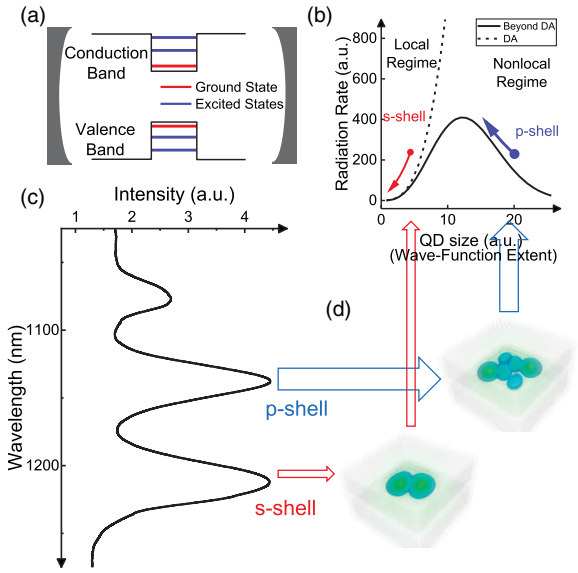

FIG. 1. (a) CQED system with a quantum emitter containing multiple excited states. (b) Radiation rate for QD with different wave-function extent under DA (dashed line) and beyond DA (solid line). Arrows show the variation of coupling strength as the wave function shrinks in a magnetic field for the s shell (red) and p shell (blue). (c) PL spectrum of ensemble QDs. The Gaussian peak at 1200 nm originates from the s shell, and the peak at 1130 nm originates from the p shell. (d) Calculated wave functions of hole states for the s shell and p shell.

confinement with the magnetic length in the plane vertical to the field [14–16]. As the magnetic field increases, the additional confinement will narrow down and shrink the wave function.

For excitons with wave-function extent much smaller than the photon wavelength, $\alpha(\boldsymbol{r})$ could be considered as a constant and taken outside the integral. Then the interaction $\boldsymbol{\alpha}\cdot\langle f|\boldsymbol{p}|i\rangle \propto \boldsymbol{\alpha}\cdot\boldsymbol{d}$ is determined by the electric dipole moment $\boldsymbol{d}=\langle f|e\boldsymbol{r}|i\rangle$, known as the DA. The dipole moment $\boldsymbol{d}$ is related to the wave-function extent. Therefore, the interaction will decay with the wave function shrinking, which has been demonstrated previously for the s-shell excitons [16,17]. However, for excitons with large wave-function extent, $\alpha(\boldsymbol{r})$ cannot be considered as a constant; thus the exciton and photon cannot be separated, and the nonlocal interaction beyond the DA becomes significant. Figure 1(b) shows the calculated nonlocal radiation rate of QDs with different sizes at the same wavelength based on the rigorous theory rather than dipole approximation or quadrupole approximation [19]. The dashed line is the result with DA, while the solid line shows the result beyond DA, and large QD size is equivalent to large wave-function extent. Although specific details may differ for various kinds of quantum emitters, the radiation rate generally will not infinitely increase with wave-function extent like the dashed line with DA. Additionally, the nonlocal effect is more significant in the cavity field [9,19]. For the radiation in homogeneous materials, the mode function of a monochromatic plane wave has a uniform density $|\boldsymbol{\alpha}(\boldsymbol{r})|^2$ with only a phase difference. While in inhomogeneous materials such as cavities, $|\boldsymbol{\alpha}(\boldsymbol{r})|$ is nonuniform. In the photonic crystal cavity, $|\boldsymbol{\alpha}(\boldsymbol{r})|$ is large in the cavity center and small away from the center. Thus, for the example of a quantum emitter in the cavity center, too large a wave-function extent obviously leads to the small coupling strength as results in Fig. 1(b), due to the small average value of $|\boldsymbol{\alpha}(\boldsymbol{r})|$.

Our sample contains a layer of self-assembled InAs QDs grown in the middle of a GaAs slab with a thickness of 170 nm. The detailed information of the sample and fabrication is in the Supplemental Material [20]. The PL spectrum of ensemble QDs with large sizes indicates three main peaks for one ground state and two excited states [Fig. 1(c)]. The s shell and p shell come from exciton recombination between the same electron state and two different hole states [34]. The hole wave function [Fig. 1(d)] of the p shell has a much larger extent than the s shell and even extends into the wetting layer [34], which can also be proved by the correlated diamagnetic shift [15] shown in Fig. 2. A few nonlocal interactions have been reported for the s shell [35]; thus a more significant nonlocal effect can be indicated from the larger wave-function extent of the p shell. Therefore, as the wave function shrinks with the magnetic field, the p-shell–cavity interaction is continuously tuned from a nonlocal regime to a local regime. And the coupling strength variation can be predicted as the blue arrow in Fig. 1(b), with the maximum value occurring during the transition between the two regimes.

When the vertical magnetic field B_z is applied, the diamagnetic shift of QD transitions is proportional to $\langle l_{\|}^2\rangle B^2$, indicating that the diamagnetism is related to the in-plane wave-function extent $l_{\|}$ [15,16,36]. Some p-shell transitions [bottom panel in Fig. 2(b)] have a diamagnetism reversal, negative below 3.5 T and positive above 3.5 T, different from other normal transitions. The reversal is difficult to explain by the Fock-Darwin model with an invariable $l_{\|}$, which gives an abnormally large effective mass from the fitting result (see the Supplemental Material [20]). In contrast, the reversal was explained with the shrinking of a large wave-function extent as demonstrated previously [37–39]. The wave-function extent of the final state can be larger than that of the initial state due to the decrease of Coulomb attraction, resulting in the redshift when the wave function of the final state extends into the wetting layer. With $B_z > 3.5$ T, however, the emission peak is blueshifted as normal with further wave-function shrinking. The diamagnetism with a horizontal magnetic field $B_{\|}$ of these transitions is also larger than the normal transitions as well [upper panel in Fig. 2(b)], indicating a large wave-function extent along the growth direction.

Due to the significant shrinking of the wave function, the coupling strength g of the p-shell–cavity system also varies

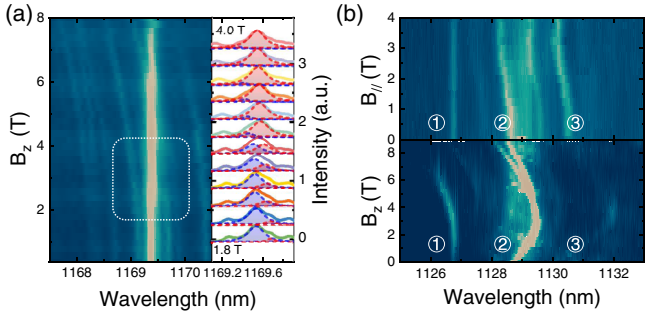

FIG. 2. (a) *Left:* PL map for *s*-shell transitions coupled to a high-Q cavity mode in B_z. *Right:* An anticrossing extracted from the dashed rectangular region in the left panel with coupling strength $g = 45$ μeV, a typical coupling strength value for *s*-shell transitions, which is relatively small compared to that for *p*-shell transitions. (b) PL map for *p*-shell transitions in a low-Q cavity mode in B_z, with diamagnetism reversal in B_z (bottom) and in $B_\parallel$ (up), correspondingly. As marked in the figure, transition 1 has a normal positive diamagnetism in B_z and a negligible diamagnetism in $B_\parallel$, while transitions 2 and 3 have a diamagnetism reversal in B_z and a relatively large diamagnetism in $B_\parallel$. The diamagnetic shift of the *p* shell is much larger than that of the *s* shell in (a), indicating a much larger wave-function extent.

with the magnetic field. In the weak coupling regime, Purcell enhanced spontaneous emission intensity of a quantum emitter in cavity radiation field with cavity mode ω_c and decay rate $\gamma_c = \omega_c/Q$ can be expressed by [40,41]

$$\gamma_{\mathrm{SE}} \propto |\langle f|\boldsymbol{\alpha}(\boldsymbol{r})\cdot\boldsymbol{p}|i\rangle|^2 D_c(\omega_x),$$

where $|\langle f|\boldsymbol{\alpha}(\boldsymbol{r})\cdot\boldsymbol{p}|i\rangle|$ is the coupling strength term, and $\pi D_c(\omega_x) = (\gamma_c/2)/[(\omega_x-\omega_c)^2+(\gamma_c/2)^2]$ is the mode density term determined by the detuning. Figure 3(a) shows the PL map of an enhanced *p*-shell transition with diamagnetism reversal in B_z. The transition is around 1 nm off resonance away from the cavity mode. The intensity of each peak is divided by the mode density $D_c(\omega_x)$ to focus

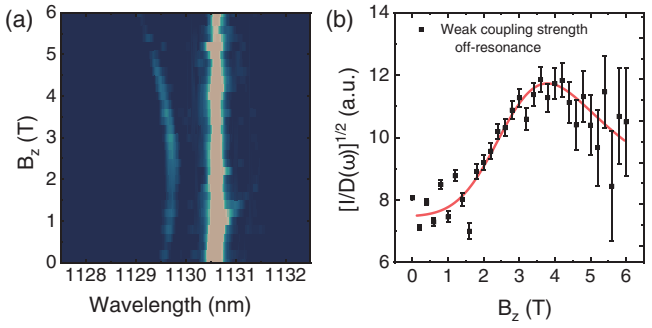

FIG. 3. (a) PL map of a *p*-shell transition with diamagnetism reversal in B_z. The transition is off resonance to the cavity mode. (b) Coupling strength variation extracted by taking the square root of $I/D(\omega)$, with the fitting results by the EMG function (red line).

on the coupling-strength term [Fig. 3(b)]. The coupling strength first increases with $B_z < 3.5$ T and then decreases with $B_z > 3.5$ T. In contrast, only the decrease of coupling strength can be predicted and observed if the DA is applied [16,17]. The increase of coupling strength directly proves the exciton-photon interaction beyond the DA, corresponding well with the nonlocal interaction model [solid line in Fig. 1(b)].

In the strong coupling regime, the Rabi splitting on resonance is [40,42]

$$\Delta E = 2\sqrt{g^2 - \left(\frac{\gamma_x - \gamma_c}{4}\right)^2},$$

from which the coupling strength g can be directly extracted. γ_x (γ_c) is the decay rate of the exciton (cavity). Figure 4 shows the PL spectra of a strongly coupled *p*-shell–cavity system. A *p*-shell transition near the cavity mode was observed with a similar reversal of diamagnetic shift and PL intensity [Fig. 4(b)], with the reversal points both around $B_z = 3.5$ T. Series of temperature tuning were applied to tune the transition and cavity to resonance, with B_z from 3 T to 5 T [upper panels in Fig. 4(a)]. Then, g values were extracted from the well-fitted results [bottom panels in Fig. 4(a)]. The variation of g [Fig. 4(c)] is in good agreement with results in the weak coupling regime (dark solid line), as expected. The maximum g at $B_z = 3.5$ T is 210 μeV (Rabi splitting of 420 μeV), much larger than the value achieved in the *s*-shell–cavity system with analogous QDs [43], and is also the largest value achieved in a cavity-dot system so far [44]. Additionally, the maximum g rapidly decays to an unobservable value with a small additional $B_\parallel = 0.5$ T (Fig. 5), indicating a high controllability related to the large wave-function extent along the growth direction. Normally, a slower decay rate of coupling strength in $B_\parallel$ was observed for excitons with smaller wave-function extent (see the Supplemental Material [20]).

The detailed calculation of a wave function in the magnetic field is nontrivial. Nonetheless, the coupling strength variation can be well explained by the wave function shrinking. The former monotonic decay of coupling strength $f_{\mathrm{decay}}(B)$ was explained with a decrease of the dipole moment as the wave function shrinks with the DA. For the *p* shell with a large wave-function extent, we extend the former monotonic decay model to a decay model with distributed delay beyond the DA. The coupling strength is $|\langle f|\boldsymbol{\alpha}(\boldsymbol{r})\cdot\boldsymbol{p}|i\rangle|$, an integration of the coupling term at different positions. Meanwhile, as B increases, the additional confinement with magnetic length $\sqrt{\hbar/eB}$ narrows down, where $\hbar$ is the reduced Planck constant and e is the elementary charge. This means that the wave function at r' starts to shrink when $B' = \hbar/er'^2$. This results in a delay of decay $f_{\mathrm{decay}}(B-B')$ for wave functions at different r' as B increases, where f_{decay} means the decay of

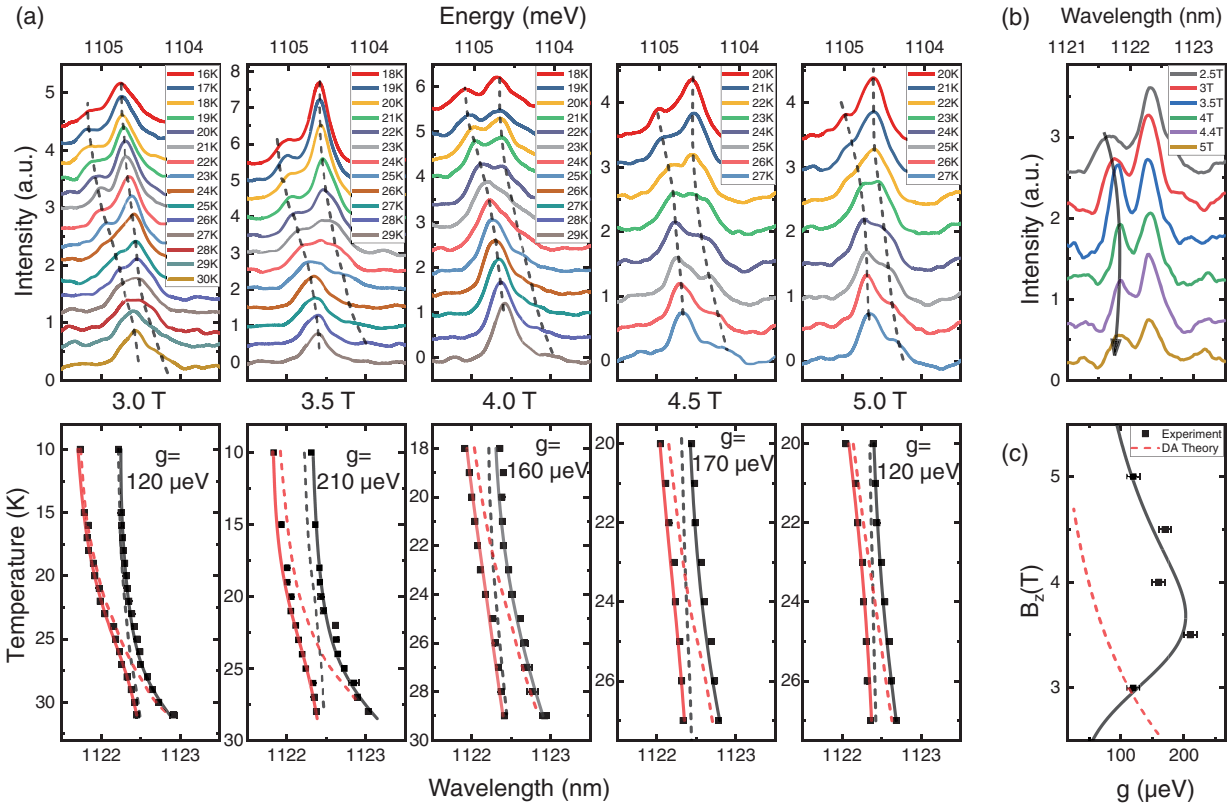

FIG. 4. (a) *Top:* Temperature-dependent PL spectra with anticrossing refer to the strong coupling between a p-shell transition and a high-Q cavity with a vertical magnetic field of 3 T, 3.5 T, 4 T, 4.5 T, and 5 T as marked in the figure. *Bottom:* Fitted peak wavelength (black dot), bare cavity and peak wavelength (dashed lines), and fitting result by the strong coupling model (solid lines) corresponding to the upper panels. The x axis is the same for each panel, with energy values shown at the top of the panel and wavelength values shown at the bottom. (b) PL spectra of the p-shell transition in a vertical magnetic field at 4.2 K. (c) Coupling strength variation extracted from Rabi splittings, in good agreement with the EMG function [black solid line; refer to Fig. 3(b)], in contrast to the theoretical model with DA [red dashed line].

the wave function in the magnetic field. Additionally, due to the nonlocal interaction, $\alpha(\boldsymbol{r})$ is nonuniform. This means that wave functions at different $\boldsymbol{r}$ have different contributions $f_{\text{distribution}}(\boldsymbol{r})$ to the coupling strength. Thus, we can have a distributed delay model

$$\begin{aligned}\hbar g(B) &= \int f_{\text{distribution}}(r') f_{\text{decay}}(B - B') dr' \\ &= \int g_{\text{distribution}}(B') f_{\text{decay}}(B - B') dB',\end{aligned}$$

where $g_{\text{distribution}}(B)$ is the transform of $f_{\text{distribution}}(\boldsymbol{r})$ in the integration with $B = \hbar/er^2$. The coupling strength variation in the experiment is well fitted by an exponentially modified Gaussian (EMG) function [solid lines in Figs. 3(b) and 4(c)]:

$$\begin{aligned}f(x) &= y_0 + (f_1 \otimes f_2)(x), \\ f_1(x) &= Ae^{-\frac{x}{\tau}}, \\ f_2(x) &= \frac{1}{\sqrt{2\pi}\sigma} e^{-\frac{(x-x_C)^2}{2\sigma^2}},\end{aligned}$$

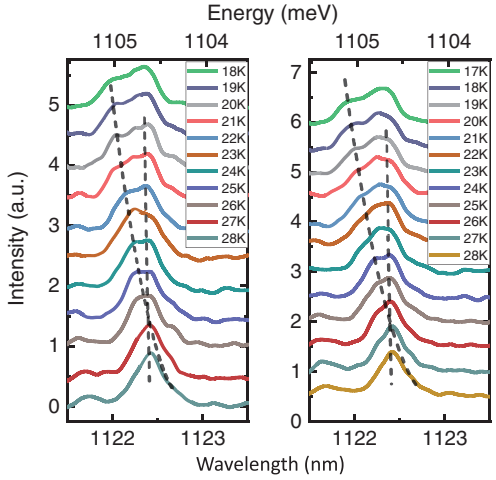

FIG. 5. Temperature-dependent PL spectra with a vector magnetic field $(B_{\parallel}, B_z)$ of (0.5 T, 3.5 T) (left) and (1.0 T, 3.5 T) (right). The interaction rapidly decays to the weak coupling regime with an additional $B_{\parallel}$.

where f_1 is an exponential decay and f_2 is a normal distribution. $f_1 \otimes f_2(x) = \int f_1(x-z) f_2(z) dz$ is the convolution of two functions. The EMG function indicates an integration of exponential decay with distributed delay, and the delay has a normal distribution of weight, corresponding well with the distributed delay model. In contrast, for s-shell transitions with the DA, $\alpha(\boldsymbol{r})$ is constant; thus wave functions at different positions have the same contribution, resulting in the degeneration back to a monotonic decrease of g, as reported previously [16]. The fitting results by the EMG function in Fig. 3(b) are $\tau = 3.7$ T as the exponential decay rate, $x_c = 2.5$ T with a corresponding magnetic length of 16 nm for the position with an average contribution to g, and $\sigma = 0.77$ T with a corresponding magnetic length of 5 nm for the standard deviation of the distribution. These values are in good agreement with the QD size. Therefore, the theoretical model well explains the coupling strength variation of both the s shell with the DA in previous works and the p shell beyond the DA in our experiment, revealing the nature of the transition between nonlocal and local interaction regimes.

In summary, we experimentally demonstrated the significant nonlocal interaction beyond the DA in the strongly coupled p-shell–cavity system and achieved a great enhancement of the coupling strength. The magnetodynamics of the exciton-photon interaction is well described by the new distributed delay model. Our work makes it possible to enhance and control the single exciton-photon interaction in solid state, which is a significant step towards the building of the quantum photonic network. Additionally, as the *in situ* wave-function control is valid for other quantum emitters as well, this work can also be extended from single exciton-photon interaction to new multidipole materials, thus benefitting various light-matter interactions such as biosensors and solar cells [45,46].

This work was supported by the National Basic Research Program of China under Grant No. 2016YFA0200400; the National Natural Science Foundation of China under Grants No. 11721404, No. 51761145104, No. 61675228, and No. 61390503; the Strategic Priority Research Program of the Chinese Academy of Sciences under Grants No. XDB07030200, No. XDB28000000, and No. XDB07020200; the Key Research Program of Frontier Sciences of CAS under Grant No. QYZDJ-SSW-SLH042; the Instrument Developing Project of CAS under Grant No. YJKYYQ20180036 and the CAS Interdisciplinary Innovation Team. Authors would like to thank Gas Sensing Solutions Ltd. for using the MBE equipment.

*xlxu@iphy.ac.cn

[1] H. J. Kimble, Nature (London) **453**, 1023 (2008).
[2] S. Ritter, C. Nölleke, C. Hahn, A. Reiserer, A. Neuzner, M. Uphoff, M. Mücke, E. Figueroa, J. Bochmann, and G. Rempe, Nature (London) **484**, 195 (2012).
[3] R. J. Warburton, Nat. Mater. **12**, 483 (2013).
[4] S. G. Carter, T. M. Sweeney, M. Kim, C. S. Kim, D. Solenov, S. E. Economou, T. L. Reinecke, L. Yang, A. S. Bracker, and D. Gammon, Nat. Photonics **7**, 329 (2013).
[5] R. Bose, T. Cai, K. R. Choudhury, G. S. Solomon, and E. Waks, Nat. Photonics **8**, 858 (2014).
[6] W. D. Heiss, J. Phys. A **45**, 444016 (2012).
[7] Y. Choi, S. Kang, S. Lim, W. Kim, J.-R. Kim, J.-H. Lee, and K. An, Phys. Rev. Lett. **104**, 153601 (2010).
[8] T. Karzig, C.-E. Bardyn, N. H. Lindner, and G. Refael, Phys. Rev. X **5**, 031001 (2015).
[9] P. Lodahl, S. Mahmoodian, and S. Stobbe, Rev. Mod. Phys. **87**, 347 (2015).
[10] G. Günter, A. A. Anappara, J. Hees, A. Sell, G. Biasiol, L. Sorba, S. De Liberato, C. Ciuti, A. Tredicucci, A. Leitenstorfer, and R. Huber, Nature (London) **458**, 178 (2009).
[11] M. D. Birowosuto, A. Yokoo, G. Zhang, K. Tateno, E. Kuramochi, H. Taniyama, M. Takiguchi, and M. Notomi, Nat. Mater. **13**, 279 (2014).
[12] P. Peng, Y.-C. Liu, D. Xu, Q.-T. Cao, G. Lu, Q. Gong, and Y.-F. Xiao, Phys. Rev. Lett. **119**, 233901 (2017).
[13] W. Gao, X. Li, M. Bamba, and J. Kono, Nat. Photonics **12**, 362 (2018).
[14] T. Schmidt, M. Tewordt, R. H. Blick, R. J. Haug, D. Pfannkuche, K. v. Klitzing, A. Förster, and H. Lüth, Phys. Rev. B **51**, 5570 (1995).
[15] S. N. Walck and T. L. Reinecke, Phys. Rev. B **57**, 9088 (1998).
[16] S. Reitzenstein, S. Münch, P. Franeck, A. Rahimi-Iman, A. Löffler, S. Höfling, L. Worschech, and A. Forchel, Phys. Rev. Lett. **103**, 127401 (2009).
[17] H. Kim, T. C. Shen, D. Sridharan, G. S. Solomon, and E. Waks, Appl. Phys. Lett. **98**, 091102 (2011).
[18] A. Faraon, A. Majumdar, H. Kim, P. Petroff, and J. Vučković, Phys. Rev. Lett. **104**, 047402 (2010).
[19] S. Stobbe, P. T. Kristensen, J. E. Mortensen, J. M. Hvam, J. Mørk, and P. Lodahl, Phys. Rev. B **86**, 085304 (2012).
[20] See Supplemental Material http://link.aps.org/supplemental/10.1103/PhysRevLett.122.087401 for the description of theoretical calculations, experimental details and more experimental data on coupling strength control, which includes Refs. [21–33].
[21] P. W. Langhoff, S. T. Epstein, and M. Karplus, Rev. Mod. Phys. **44**, 602 (1972).
[22] R. Fitzpatrick, *Quantum Mechanics* (World Scientific, Singapore, 2015).
[23] A. Ludwig, J. Maurer, B. W. Mayer, C. R. Phillips, L. Gallmann, and U. Keller, Phys. Rev. Lett. **113**, 243001 (2014).
[24] G. Klimeck, M. Korkusinski, H. Xu, S. Lee, S. Goasguen, and F. Saied, in *5th IEEE Conference on Nanotechnology, Nagoya, Japan, 2005* (IEEE, New York, 2005), Vol. 2, pp. 807.
[25] L. Wang and A. Zunger, J. Chem. Phys. **100**, 2394 (1994).
[26] E. T. Jaynes and F. W. Cummings, Proc. IEEE **51**, 89 (1963).
[27] T. Yoshie, A. Scherer, J. Hendrickson, G. Khitrova, H. M. Gibbs, G. Rupper, C. Ell, O. B. Shchekin, and D. G. Deppe, Nature (London) **432**, 200 (2004).

[28] J. P. Reithmaier, G. Sek, A. Löffler, C. Hofmann, S. Kuhn, S. Reitzenstein, L. V. Keldysh, V. D. Kulakovskii, T. L. Reinecke, and A. Forchel, Nature (London) **432**, 197 (2004).
[29] E. M. Purcell, H. C. Torrey, and R. V. Pound, Phys. Rev. **69**, 37 (1946).
[30] H. Kim, D. Sridharan, T. C. Shen, G. S. Solomon, and E. Waks, Opt. Express **19**, 2589 (2011).
[31] Y. Akahane, T. Asano, B.-S. Song, and S. Noda, Nature (London) **425**, 944 (2003).
[32] J. Jimenez-Mier, J. Quant. Spectrosc. Radiat. Transfer **51**, 741 (1994).
[33] A. Babinski, M. Potemski, S. Raymond, J. Lapointe, and Z. R. Wasilewski, Phys. Rev. B **74**, 155301 (2006).
[34] O. Stier, M. Grundmann, and D. Bimberg, Phys. Rev. B **59**, 5688 (1999).
[35] M. L. Andersen, S. Stobbe, A. S. Sørensen, and P. Lodahl, Nat. Phys. **7**, 215 (2011).
[36] C. Schulhauser, D. Haft, R. J. Warburton, K. Karrai, A. O. Govorov, A. V. Kalameitsev, A. Chaplik, W. Schoenfeld, J. M. Garcia, and P. M. Petroff, Phys. Rev. B **66**, 193303 (2002).
[37] Y. J. Fu, S. D. Lin, M. F. Tsai, H. Lin, C. H. Lin, H. Y. Chou, S. J. Cheng, and W. H. Chang, Phys. Rev. B **81**, 113307 (2010).
[38] S. Cao, J. Tang, Y. Gao, Y. Sun, K. Qiu, Y. Zhao, M. He, J.-A. Shi, L. Gu, D. A. Williams, W. Sheng, K. Jin, and X. Xu, Sci. Rep. **5**, 8041 (2015).
[39] S. Cao, J. Tang, Y. Sun, K. Peng, Y. Gao, Y. Zhao, C. Qian, S. Sun, H. Ali, Y. Shao, S. Wu, F. Song, D. A. Williams, W. Sheng, K. Jin, and X. Xu, Nano Res. **9**, 306 (2016).
[40] L. C. Andreani, G. Panzarini, and J.-M. Gérard, Phys. Rev. B **60**, 13276 (1999).
[41] D. Englund, D. Fattal, E. Waks, G. Solomon, B. Zhang, T. Nakaoka, Y. Arakawa, Y. Yamamoto, and J. Vučković, Phys. Rev. Lett. **95**, 013904 (2005).
[42] K. Hennessy, A. Badolato, M. Winger, D. Gerace, M. Atatüre, S. Gulde, S. Fält, E. L. Hu, and A. Imamoglu, Nature (London) **445**, 896 (2007).
[43] C. Qian, S. Wu, F. Song, K. Peng, X. Xie, J. Yang, S. Xiao, M. J. Steer, I. G. Thayne, C. Tang, Z. Zuo, K. Jin, C. Gu, and X. Xu, Phys. Rev. Lett. **120**, 213901 (2018).
[44] Y. Ota, D. Takamiya, R. Ohta, H. Takagi, N. Kumagai, S. Iwamoto, and Y. Arakawa, Appl. Phys. Lett. **112**, 093101 (2018).
[45] G. Kim, B. Walker, H. Kim, J. Y. Kim, E. H. Sargent, J. Park, and J. Y. Kim, Adv. Mater. **26**, 3321 (2014).
[46] P. Alivisatos, Nat. Biotechnol. **22**, 47 (2004).